https://doi.org/10.5194/egusphere-2025-4874
Preprint. Discussion started: 15 October 2025

Global hotspots and mechanisms of extreme humid heat and air pollution co-occurrence

Samuel Bartusek[1,2], Yutian Wu[1,2], Mingfang Ting[1,3], Arlene Fiore[4], and Daniel M. Westervelt[1,2]

[1]Columbia University
[2]Lamont-Doherty Earth Observatory
[3]Columbia University Climate School
[4]Massachusetts Institute of Technology

Correspondence: Samuel Bartusek (samuel.bartusek@columbia.edu)

Abstract.

Exposure to extreme humid heat and air pollution each represent significant, well-characterized environmental hazards to human health. But the questions of where, when, and why they may co-occur, and whether humid heat may exacerbate pollution relative to high temperatures alone, remain largely unexplored. Here, we identify regions worldwide where ozone (O_3) or particulate matter ($PM_{2.5}$) pollution tend to be higher during humid versus non-humid extreme heat—i.e., where increased moist heat stress tends to co-occur with increased pollution, revealing a compound hazard tendency—and characterize the meteorological and chemical drivers of this co-occurrence. We analyze 19 years of near-surface concentrations of ozone, $PM_{2.5}$, and related species (NO_2 and HCHO) in the Copernicus Atmosphere Monitoring Service global chemical reanalysis (CAMSRA), along with meteorological conditions from the European Centre for Medium-Range Weather Forecasts Reanalysis version 5 (ERA5). We find that the global hotspots of worsened pollution during humid heat overlap with several global hotspots of extreme humid heat itself, and include multiple densely-populated areas. Altogether, more of the global population experiences worsened air quality during humid heat (versus dry heat) than experiences cleaner air quality. Overall, we find that humid heat and pollution co-occurrence hotspots typically occur where (1) the near-surface background chemical makeup is more urban (higher NO_2, lower HCHO), and (2) humid heat is associated with stagnation and suppressed boundary layer heights (as is common in areas that experience severe humid heat), such that the local meteorological drivers of extreme humid heat are also conducive to pollutant accumulation.

1 Introduction

Extreme heat can be harmful to human, agricultural, and ecological health, with thousands of premature deaths per year worldwide linked to high temperatures (Basu and Samet, 2002; Gasparrini et al., 2015; Lesk et al., 2016; Weinberger et al., 2020; Ballester et al., 2023). Under global warming, exposure to extreme heat has increased and will intensify further, with growing morbidity and mortality impacts (Mora et al., 2017; Huang et al., 2011; Meehl and Tebaldi, 2004). A growing body of research has characterized the role of moisture in the severity of extreme heat's health impacts, as higher humidity during extreme heat events hinders evaporative cooling via perspiration (Sherwood and Huber, 2010; Vecellio et al., 2022, 2023;

https://doi.org/10.5194/egusphere-2025-4874
Preprint. Discussion started: 15 October 2025

Raymond et al., 2020; Mora et al., 2017). Metrics combining temperature and humidity, such as wet-bulb temperature, therefore measure physiological heat stress better than temperature alone (Haldane, 1905; Vecellio et al., 2022). Extreme humid heat increases faster under global warming than extreme temperatures alone, and exposure has disproportionately increased in populated areas, especially in the tropics (Rogers et al., 2021; Matthews et al., 2022; Speizer et al., 2022). Wet-bulb temperature levels thought to be physiologically uncompensable (i.e., fatal under sustained exposure) that have likely only occurred for a few hours at a time in a few locations in the recent climate are projected to become rapidly more frequent, potentially occurring for hundreds of hours per year across widespread areas of the tropics and subtropics, depending on future warming levels (Pal and Eltahir, 2016; Raymond et al., 2020; Vecellio et al., 2023).

Recent work has revealed distinct meteorological drivers of humid heat events, as compared to heatwaves measured by temperature alone (Raymond et al., 2017, 2021). While non-humid heatwaves are often driven by large-scale anticyclonic circulation and high solar radiation, humid heat events typically require a build-up of moisture in the boundary layer, via horizontal advection or evaporation, that is allowed to become extreme by mechanisms suppressing the triggering of convection (Horton et al., 2016; Barriopedro et al., 2023; Raymond et al., 2021; Duan et al., 2024). Such conditions usually occur on small spatial scales, and the particular drivers of humid heat can vary significantly between locations. The most extreme humid heat conditions worldwide typically occur in subtropical latitudes, near plentiful moisture sources: notable hotspots include the coastline around the Persian Gulf and highly-irrigated land along the Indo-Gangetic plain in South Asia (Raymond et al., 2021; Duan et al., 2024; Ivanovich et al., 2022; Im et al., 2017).

Near-surface air pollution is also a significant threat to human health, responsible for millions of premature deaths per year (Lelieveld et al., 2015; Cohen et al., 2005; Pope III et al., 2002). Overall, exposure to air pollution is projected to increase over the 21st century due to both population growth and worsened pollution in polluted areas, even though pollution has been markedly improving in many areas globally (Pozzer et al., 2024; Li et al., 2023). For instance, under a high-emissions trajectory, extreme pollution episodes in South Asia may increase dramatically, with concentrations of particulate matter less than 2.5 μm in diameter ($PM_{2.5}$) breaching World Health Organization (WHO) air quality guidelines nearly daily by 2050 (Kumar et al., 2018). In the absence of emissions changes, global warming (and associated surface moistening) is expected to decrease baseline surface ozone (O_3) over much of the globe, but increase it (largely through increased stagnation) in polluted areas such as North America, Europe, and East and South Asia, especially during the summer (Jacob and Winner, 2009; Zanis et al., 2022; Fu and Tian, 2019; Fiore et al., 2012, 2015). In East Asia, strong air quality improvements in terms of particulate pollution since 2013 have been coupled with rapid increases in ozone pollution, indicating non-linear interactions between gases and particles (Li et al., 2019; Lu et al., 2018; Zhai et al., 2019; Gopikrishnan et al., 2025).

Recent research has investigated extreme heat and air pollution as compounding hazards, in terms of both impacts and mechanisms. Epidemiological evidence suggests that the co-occurrence of heat and pollution hazards can synergistically compound their health impacts far above the additive effect of each individually (Rahman et al., 2022; Anenberg et al., 2020; Willers et al., 2016). High temperatures can increase the production of ozone in the near-surface atmosphere both directly, by increasing the rate of its photochemical formation from precursor species (volatile organic compounds [VOCs] and nitrogen oxides [NO_x]), and indirectly, by increasing the emission of biogenic precursors themselves (VOCs) from plants (Camalier et al., 2007; Dun-

https://doi.org/10.5194/egusphere-2025-4874
Preprint. Discussion started: 15 October 2025

can et al., 2009; Guenther et al., 1993; Sillman and Samson, 1995). Additionally, the meteorological conditions that accompany high temperatures can also contribute to increased ozone: high solar radiation can further amplify its photochemical production and stagnant conditions can hinder its dispersal from the boundary layer (Jacob et al., 1993; Porter and Heald, 2019). The sensitivity of $PM_{2.5}$ to temperature is more complex (Tai et al., 2010), with different components of the particulate matter mix reacting differently, though lack of cloud cover and stagnation both can enhance $PM_{2.5}$, potentially even more strongly than ozone (Jacob and Winner, 2009; Dawson et al., 2014; Pye et al., 2009; Westervelt et al., 2016). Consequently, heatwaves often coincide with high-ozone and high-$PM_{2.5}$ episodes, as demonstrated in eastern North America by Schnell and Prather (2017).

However, there is limited understanding of how variability in humidity during extreme heat affects ozone and particulate pollution. Ozone is known to be strongly associated with (low) relative humidity, partially through a direct mechanism of reduced dry deposition via plants but partially due to the underlying correlation of high temperature and low relative humidity (Kavassalis and Murphy, 2017). Its relationship with specific humidity is more complex and spatially variable, with positive correlations found over much of midlatitude land, related more to transport than chemical processes (Kerr et al., 2020). Particulate matter may be increased by humidity through hygroscopic growth of aerosol particles, though there is a lack of research focusing on high temperature conditions (Cheng et al., 2015). Regional studies have documented that during summer in Beijing, humid heat is highly coupled with ozone and $PM_{2.5}$ concentrations due to stagnation and suppressed boundary layer heights (Miao et al., 2022), and that across South Asia, joint occurrences of extreme humid heat and particulate pollution may increase substantially in the 21st century (Xu et al., 2020). But a systematic global-scale investigation of the co-occurrence between humid heat stress—rather than just high temperatures—and air pollution is lacking.

Here, we compare near-surface pollution during humid versus non-humid heat extremes, across global land area. We analyze near-surface ozone and $PM_{2.5}$ concentrations in the Copernicus Atmosphere Monitoring Service global chemical reanalysis (CAMSRA) over the period 2003–2021. In hotspots of humid heat and pollution co-occurrence, we validate CAMSRA data against U.S. Embassy in-situ observations where possible, and we analyze near-surface meteorological fields from the European Centre for Medium-Range Weather Forecasts Reanalysis v5 (ERA5). We show that in many regions worldwide, during extreme heat conditions, increased humidity corresponds with worsened pollution, and we investigate the meteorological and chemical drivers of this humid heat and air pollution co-occurrence.

2 Data and Methods

2.1 Datasets and variables

In this study we analyze several meteorological variables from the state-of-the-art high-resolution (0.25°) European Centre for Medium-Range Weather Forecasts (ECMWF) Reanalysis version 5 (ERA5) (ERA5; Hersbach et al., 2020). We calculate daily-maximum temperature (T_{max}) and wet-bulb temperature (TW_{max}) at 2 meter elevation from hourly timesteps, and daily-mean 2-meter dewpoint temperature, 10-meter wind components, and boundary-layer height, over the years 2003–2021, with the 1981–2010 period also analyzed for T_{max} and TW_{max} to calculate extreme heat thresholds (see below).

https://doi.org/10.5194/egusphere-2025-4874
Preprint. Discussion started: 15 October 2025

We additionally analyze several chemical species from the ECMWF's Copernicus Atmosphere Monitoring Service global chemical reanalysis CAMSRA (Inness et al., 2019), which is an ideal dataset as it provides a long-term, consistent, global-scale estimate of real-world atmospheric composition. CAMSRA assimilates satellite retrievals of trace gases and aerosols and incorporates a chemical transport model, and extends from 2003 to the near-present at 3-hourly and 0.75° resolution. In CAMSRA, meteorological fields are produced by a very similar version of ECMWF's Integrated Forecasting System (IFS; cycle 42R1) as ERA5 (cycle 41R2), with tropospheric chemistry calculated online by the Carbon Bond 2005 chemical mechanism (CB05; Flemming et al., 2015). In CAMSRA, anthropogenic emissions are based on the MACCity inventory (Granier et al., 2011), monthly-mean biogenic emissions are derived from a dataset of hourly calculations by the Model of Emissions of Gases and Aerosols from Nature, version 2.1 (MEGANv2.1), forced by meteorology from NASA's Modern-Era Retrospective Analysis for Research and Applications (MERRA) reanalysis (Guenther et al., 1995, 2006; Sindelarova et al., 2014). Daily biomass burning emissions data are provided by the Global Fire Assimilation System version 1.2 (GFASv1.2; Kaiser et al., 2012). From CAMSRA we calculate daily-maximum O_3 and daily-mean $PM_{2.5}$, NO_2, and HCHO at the lowest model level, over the years 2003–2021.

2.2 Validation of chemical reanalysis data

Overall, CAMSRA has been found to provide an accurate representation of reactive gases on a global scale that improved upon previous generations of chemical reanalysis (Wagner et al., 2021). Studies comparing surface-level ozone and/or particulate matter from CAMSRA against a variety of observational sources worldwide have found generally significant mean-state biases but relatively good correspondence of shorter-term temporal variability, typically outperforming other chemical reanalyses. On a daily scale, moderate to high temporal correlations with observations were found for ozone and $PM_{2.5}$ in Europe ($r = 0.61$ and 0.43 respectively, over 2003–2020; Lacima et al. (2023)), for ozone and PM_{10} in South Korea ($r = 0.8$ and 0.74 respectively, over 2003–2018; Ryu and Min (2021)), for ozone in the United States (r ranging from 0.53 to 0.89 across regions, over 2014; Williams et al. (2022)), for $PM_{2.5}$ in China ($r = 0.56$, over 2014–2020; Ali et al. (2022)), and for $PM_{2.5}$ globally ($r = 0.6$, over 2017–2019; Jin et al. (2022)), despite widespread mean biases in absolute values.

Since our analysis is based on anomalies (daily-scale differences from climatological seasonal cycles), it focuses on the synoptic-scale variations that CAMSRA performs better for, and is likely minimally affected by its mean-state biases. Additionally, for the selected hotspots we focus on, we compare CAMSRA data against AirNow U.S. Embassy measurements if available. Figures S1–S6 show comparisons for ozone and $PM_{2.5}$ in Beijing, $PM_{2.5}$ in Shanghai, ozone and $PM_{2.5}$ in Guangzhou, and $PM_{2.5}$ in Islamabad, generally showing moderate correlations between observed and simulated daily anomalies (despite sometimes large differences in climatologies) and agreement in the sign of differences between humid and non-humid heat conditions, except where the small sample size of overlapping observations prevents such a quantitative comparison (Figure S4).

https://doi.org/10.5194/egusphere-2025-4874
Preprint. Discussion started: 15 October 2025

2.3 Methods

We define extreme non-humid (hereafter, "dry") and humid heat days (for individual ERA5 gridcells) as days during which, respectively, either *only* T_{max} (but *not* TW_{max}) or *both* T_{max} and TW_{max} exceed their 95th percentile value over the 1981–2010 period (see schematic in Figure 1). The difference in temperature between humid and dry heat days defined in this way is much smaller than that between days in which T_{max} and TW_{max} are individually extreme regardless of the other (Figure S7). Therefore, the comparison of humid versus dry heat days on average represents an increase in moisture for roughly constant temperature, corresponding more directly to an increase in heat stress, and largely de-emphasizing contributions of temperature change to differences in pollutant concentrations (Figure S7). Throughout the analysis, we exclude gridcells where (1) the average TW_{max} of humid heat days is in the lowest quartile of all land area, in order to concentrate on areas of relatively significant humid heat exposure; or (2) the total number of humid heat days is fewer than 1% of all extreme-T_{max} days in the same location, in order to ensure adequate sample size of comparison groups. The union of these excluded gridcells is shaded gray in Figures 1 and 2.

For all meteorological and chemical variables, we analyze anomalies relative to a daily climatology calculated at each gridcell (the mean for each calendar day calculated across the 2003–2021 period and smoothed with a 30-day moving window average around the calendar), with the linear trend in the anomalies' daily time series over 2003–2021 removed. When variables on the CAMSRA grid (0.75°) are analyzed during dry or humid heat days, which are defined on the ERA5 grid (0.25°), the ERA5 grid cell at the center of each CAMSRA grid cell (i.e., that with the matching longitude and latitude coordinate) is used to define the days of interest. However, for the more detailed analysis of selected hotspot locations (composites in Figures 4 and 5 and driver analysis in Figure 6), for two locations (Islamabad and Allahabad) that experience a low number of humid heat days relative to dry heat days, dry and humid heat days for CAMSRA variables are defined as those in which *any* of the 9 ERA5 grid cells within the local CAMSRA grid cell experience a dry or humid heat day, respectively, in order to increase the sample size.

For significance testing of the differences in variables between dry and humid heat days in hotspot locations, we perform a bootstrapping procedure, since the sample size of each group of days can be quite different. Each group of days is resampled 1,000 times with replacement (drawing the original number of samples), and the difference between each group's mean is computed each time. If the 2.5th and 97.5th percentiles of the distribution of 1,000 differences do not cross zero, the difference is considered statistically significant. This procedure is applied at each gridcell individually within the region (with respect to the dry and humid heat days of just the central gridcell), for each variable in the regional composite differences shown in the third column of Figures 4 and 5.

https://doi.org/10.5194/egusphere-2025-4874
Preprint. Discussion started: 15 October 2025

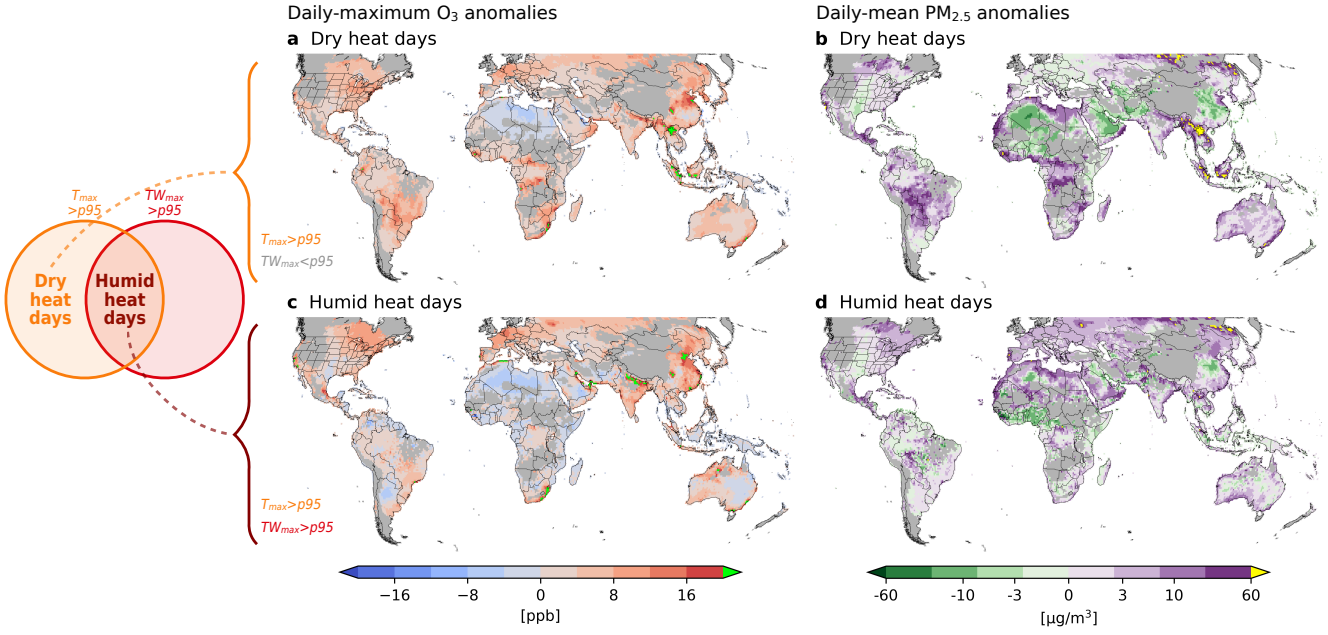

Figure 1. Ozone and particulate pollution during dry and humid extreme heat. a: Anomalies of daily-maximum ground-level O_3 concentration in the global chemical reanalysis CAMSRA during days with daily-maximum temperature exceeding its local long-term 95th percentile value and daily-maximum wet-bulb temperature *not* exceeding its 95th percentile, averaged over 2003–2021. Land area with very low humid heat exposure or very little overlap between extreme temperature and extreme wet-bulb temperature days is shaded gray. See Data and Methods for details. **b:** Same as **a**, but for anomalies of daily-mean $PM_{2.5}$. **c–d:** Same as **a–b**, but for days with daily-maximum temperature and daily-maximum wet-bulb temperature *both* exceeding their 95th percentile. Humid versus dry heat therefore mostly represents a difference in humidity, not temperature (see Data and Methods).

3 Results

3.1 Global distribution of pollution during humid versus dry heat and co-occurrence hotspots

In Figure 1 we compare reanalysis-derived ground-level pollution concentrations during extreme dry heat versus extreme humid heat conditions, across global land area. During both extreme dry and humid heat, pollution anomalies are positive over much of the globe, though with variation. On dry heat days (Figure 1a–b), both O_3 and $PM_{2.5}$ anomalies are especially high in tropical-to-subtropical locations, notably in central South America, central and southern Africa, the Ganges River plain, mainland and maritime southeast Asia, and eastern coastal Australia. Additional hotspots of O_3 include midlatitude locations such as the eastern U.S., northern Europe, and eastern coastal China, while $PM_{2.5}$ hotspots also include coastal northern and northwest Africa and eastern Russia. On humid heat days, many strong hotspots of dry heat pollution disappear—however, hotspots of pollution unique to humid heat days become evident—for instance, O_3 surrounding the Persian Gulf, and $PM_{2.5}$ in eastern coastal China. In the following, we further investigate the global pattern of the different pollution levels during

https://doi.org/10.5194/egusphere-2025-4874
Preprint. Discussion started: 15 October 2025

dry and humid heat, as well as selected hotspots where an increase in heat stress tends to co-occur with increased pollution concentrations.

Figure 2 reveals, across global land area, regional hotspots where pollution anomalies are higher during humid heat days than dry heat days. The global pattern of the pollution difference between humid and dry heat is fairly heterogeneous; in addition to distinct regional hotspots of increased pollution during humid heat, areas of suppressed pollution are also evident. Overall, increased pollution during humid heat is seen across much of the Northern Hemisphere land area, for both O_3 and $PM_{2.5}$. Strong localized hotspots of co-occurrence tend to cluster in the Northern Hemisphere subtropics, with many located close to coastlines. We note that locations at subtropical latitudes and proximal to plentiful moisture sources are thought to be those most at-risk for extreme humid heat (Raymond et al., 2021), heightening the potential health impacts of this identified co-occurrence. Additionally, we note that the large-scale distributions of co-occurrence values for O_3 and $PM_{2.5}$ individually are quite similar (spatial correlation of $r = 0.54$)—this signals that the impacts more likely compound rather than offset between the two pollutants, and implies that the mechanisms generally driving co-occurrence are fairly consistent between between them and perhaps somewhat related to meteorological differences rather than distinct chemical processes.

To begin to mechanistically investigate the phenomenon of humid heat and pollution co-occurrence, we first select hotspot regions (for each pollutant) to analyze in further detail, as outlined with dashed boxes in Figure 2a,c. Given that the distribution of co-occurrence strength is widespread and heterogeneous, we focus on areas of a strong, geographically-coherent positive anomaly difference (red or purple, or especially bright green or yellow pixels in Figure 2a,c) that also have notably high anomaly during humid heat as highlighted in Figure 1c–d (e.g., excluding areas such as the Chengdu–Chongqing urban agglomeration), are highly-populated (e.g., excluding the northern coastline of the North American Great Lakes), and contain sufficient land pixels (e.g., excluding the northern coastline of Algeria). We note that many of the selected hotspots for O_3 and $PM_{2.5}$ individually are in fact hotspots of both together (comparing Figure 2a and c), potentially suggesting the importance of shared meteorological or chemical mechanisms. Furthermore, many of these hotspot regions are in common with areas of the globally most-extreme humid heat exposure, most notably surrounding the Persian Gulf and in northern Pakistan (Raymond et al., 2021). These hotspots are examined individually and in a broader context in Figures 4, 5, and 6.

Finally, we note that many global hotspots of co-occurrence occur in highly-populated areas. For example, O_3 anomalies are over 15 ppb higher on humid versus dry heat days (bright green pixels) in regions such as the Persian Gulf, northwest India along the Ganges, and along eastern coastal China where its population is concentrated; $PM_{2.5}$ anomalies are over 30 $\mu g/m^3$ higher during humid heat in the aforementioned regions and additionally in northern Pakistan and surrounding Moscow—although areas of high co-occurrence also include sparsely-populated regions such as the Sahara and Arabian Deserts. Additionally, for both O_3 and $PM_{2.5}$, some of the most notable regions of strong positive anomalies during dry heat days (Figure 1) are shown here to experience much lower pollution during humid heat days (negative differences), including parts of central South America, central Africa, and both mainland and maritime southeast Asia. Notably, these are sparsely-populated and intensely-vegetated regions. In Figure 2b,d we compare the distribution of population versus land area across co-occurrence values, which confirms quantitatively that for both O_3 and $PM_{2.5}$, a greater portion of population than of land area is exposed to co-occurrence. Altogether (outside of the gray masked areas), 55% of the population, versus 31% of the land

https://doi.org/10.5194/egusphere-2025-4874
Preprint. Discussion started: 15 October 2025

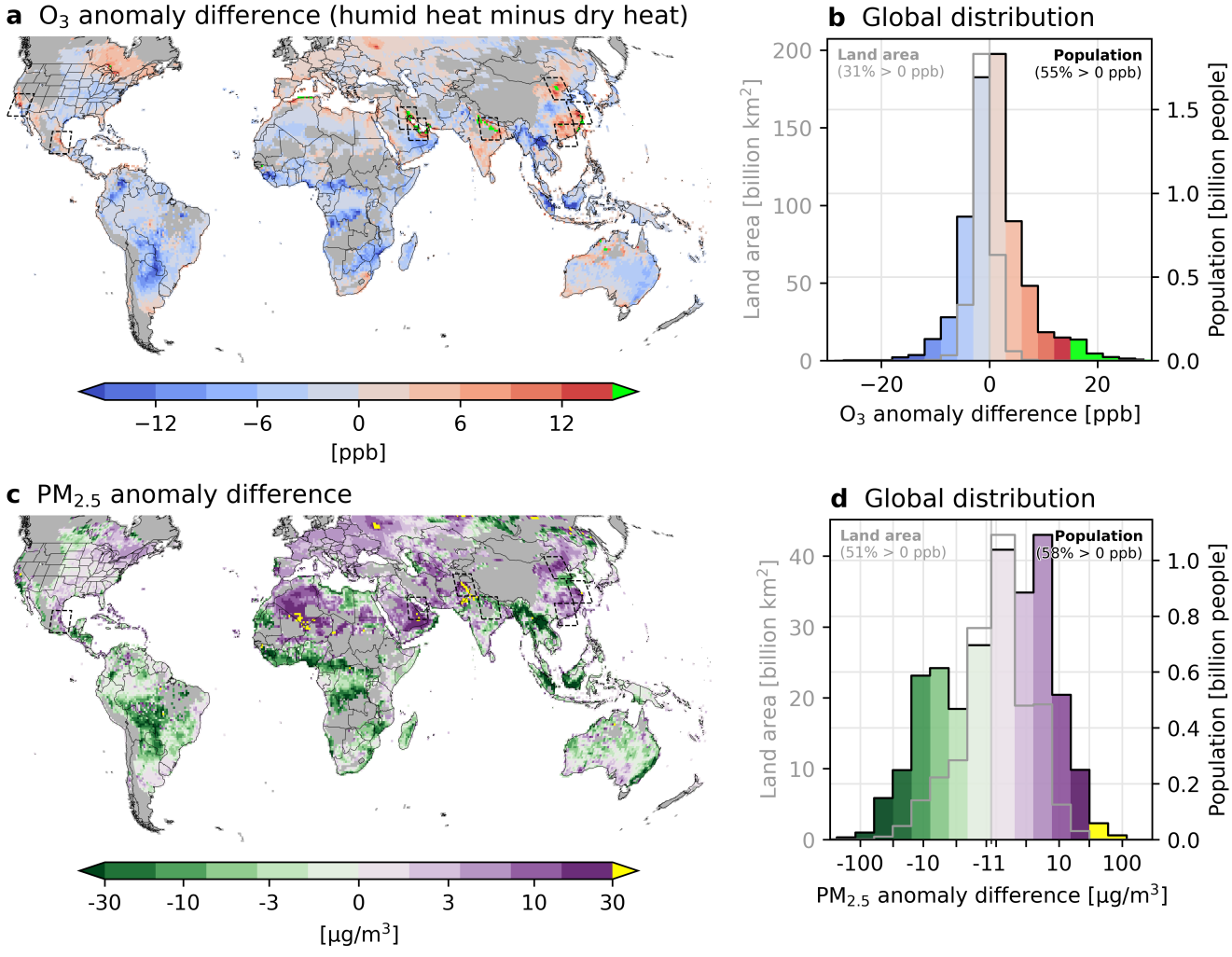

Figure 2. Difference in pollution between dry and humid extreme heat across global land area and population. a: Mean anomalies of daily-maximum ground-level O_3 during humid heat days minus those during dry heat days, over 2003–2021 (i.e., Figure 1 panel **c** minus **a**). Areas where O_3 anomalies during humid heat is over 15 ppb higher than during dry heat are highlighted in bright green; hotspot regions selected for further analysis are outlined in dashed rectangles. Excluded grid cells are colored gray as in Figure 1 **b:** *Left y-axis, gray histogram:* Distribution of O_3 differences between humid and dry heat days (i.e., values in **a**) across non-excluded land area. *Right y-axis, black histogram (colored according to **a**):* Distribution of O_3 differences across population (within non-excluded land area), highlighting the disproportionate impact of higher pollution during humid heat days in populated areas versus all land area. **c–d:** Same as **a–b** but for anomalies of daily-mean $PM_{2.5}$, with areas highlighted in yellow where $PM_{2.5}$ is over 30 $\mu g/m^3$ higher during humid heat than dry heat, and selected hotspots for $PM_{2.5}$ shown.

https://doi.org/10.5194/egusphere-2025-4874
Preprint. Discussion started: 15 October 2025

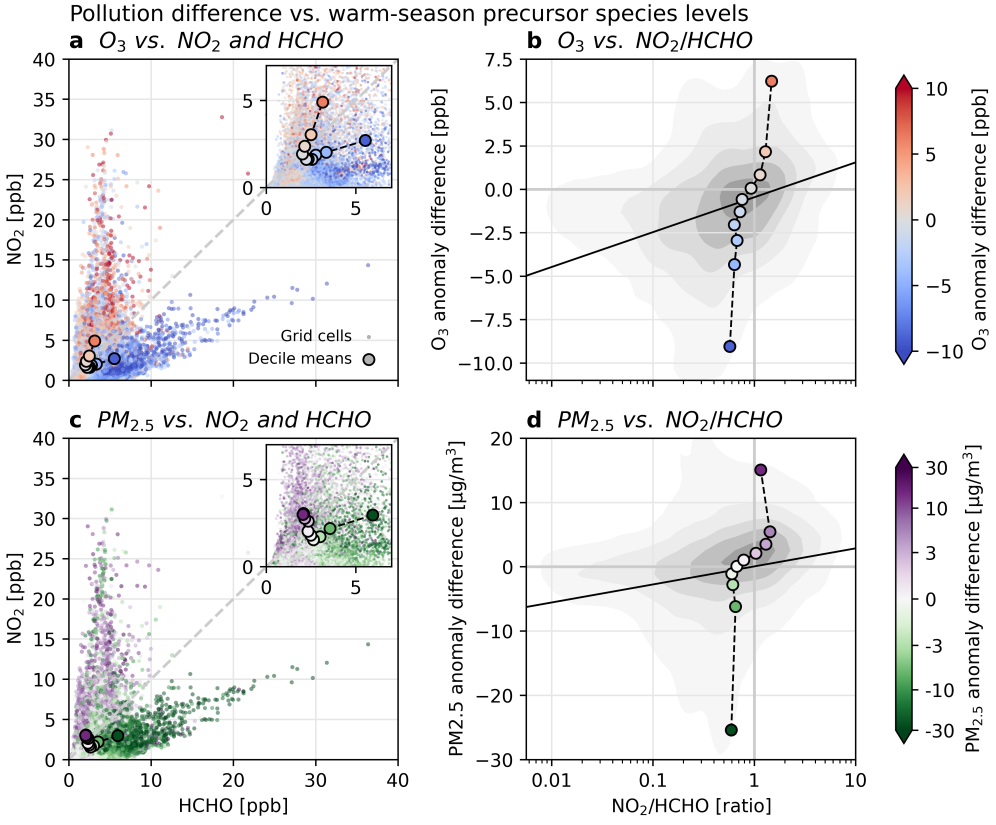

Figure 3. Dependence of humid heat and pollution co-occurrence on background chemistry regime. a: Mean O_3 anomaly differences between humid and dry heat days over 2003–2021 (values in Figure 2**a**; positive values indicate a co-occurrence tendency) are plotted in color against local warm-season mean formaldehyde (HCHO) on the *x*-axis and nitrogen dioxide (NO_2) on the *y*-axis; each small dot represents one grid cell. Large dots show the mean of each area-weighted decile of O_3 differences, plotted against their mean HCHO and NO_2; see inset for magnified view. The gray dashed line indicates equal HCHO and NO_2. **b:** The same O_3 anomaly differences are plotted on the *y*-axis against the ratio of warm-season mean NO_2 and HCHO instead of each separately. Gray contours summarize the distribution of grid cell points, and the black line shows its linear regression slope. Large dots show decile means of O_3, as in **a**, and NO_2/HCHO ratio. **c–d:** Same as **a–b** but for differences of $PM_{2.5}$ during humid versus dry heat.

area, is exposed to co-occurrence for O_3, and 58% versus 51% respectively for $PM_{2.5}$. (The non-masked areas represent 86% of the total global population.) In other words, the co-occurrence fields are both positively-correlated with population (albeit weakly, with spatial correlation coefficients of $r = 0.18$ for O_3 and $r = 0.03$ for $PM_{2.5}$). Besides emphasizing the population exposure of co-occurrence, this raises the question of whether there is a causal relationship underlying the correlation—i.e., if more anthropogenic near-surface chemistry regimes such as those typical of urban areas are partly responsible for the co-occurrence of pollution with humid rather than dry heat.

https://doi.org/10.5194/egusphere-2025-4874
Preprint. Discussion started: 15 October 2025

3.2 Dependence of co-occurrence on background chemistry

To more mechanistically investigate the global pattern of co-occurrence, we next show that across all global land area there exists a tendency towards stronger humid heat and pollution co-occurrence where the background chemistry regime is more typical of urban areas. Figure 3 shows the dependence of each land gridcell's strength of humid heat and pollution co-occurrence on its average HCHO and NO_2 over the local warm season. We define gridcell-specific warm seasons as any month wherein a dry or humid heat day (as defined in Data and Methods) occurs; they may therefore evolve over different years, and better represent background conditions for the sample of heat days we consider. HCHO and NO_2 are often used as proxies for total VOC reactivity and all NO_x species (NO + NO_2), respectively. Across land area, gridcells largely occupy either a lower-VOC and higher-NO_x regime (distributed along the *y*-axis in Figure 3a, 3c), or a higher-VOC and lower-NO_x regime (along the x-axis in Figure 3a, 3c). In lower-VOC/higher-NO_x regimes, typical of urban areas, increased VOC concentrations in the presence of abundant NO_x and sunlight allow O_3 production, and in such regions O_3 is therefore more limited by VOC than NO_x concentrations. Inversely, O_3 is NO_x-limited in lower-NO_x/higher-VOC, which are more typically remote. We find that areas where O_3 tends to be higher during humid heat than dry heat tend to be low in HCHO and high in NO_2 (Figure 3a). Additionally, across global quantiles of O_3 difference between humid and dry heat days, there is a monotonic increase in the $\frac{NO_2}{HCHO}$ ratio, indicating an overall tendency towards more NO_x-saturated background chemistry regimes where humid heat and O_3 pollution co-occurrence is stronger (Figure 3b). For $PM_{2.5}$, the relationship with background regime is similar but weaker and less monotonic; in general, the $\frac{NO_2}{HCHO}$ ratio also increases with higher $PM_{2.5}$ difference values, except in its very highest quantiles (Figure 3d). Whether this association is causal—whether a NO_x-saturated regime somehow predisposes a region to stronger humid heat and pollution co-occurrence—remains unclear and worthy of future investigation, but we provide a potential hypothesis in the Discussion.

3.3 Composite analysis of co-occurrence mechanisms in selected hotspot regions

We next examine the regional-scale drivers of humid heat and pollution co-occurrence, showing that in selected hotspot regions during dry versus humid heat the associated meteorological conditions and pollutant precursor compositions follow distinct patterns. For two hotspot regions, respectively exemplifying strong co-occurrence of humid heat with O_3 and with $PM_{2.5}$ pollution, we construct composites of typical meteorological and chemical conditions at regional scale when extreme dry and humid heat conditions occur at the center of the region. First, the Persian Gulf region displays some of the strongest humid heat and O_3 co-occurrence worldwide, with Kuwait City a notable locus (Figure 2a), as well as experiencing some of the most extreme humid heat worldwide (Raymond et al., 2021). Figure 4 shows that on dry heat days in Kuwait City (defined at the specific gridcell, not regionally), weakly negative O_3 anomalies are seen centering on the city, with some positive anomalies to the southeast over the Persian Gulf and its adjacent land. On humid heat days a reversed pattern is seen, with the strongest O_3 anomalies (> 30 ppb) centering slightly offshore. In the Kuwait City gridcell, O_3 anomalies are ~ 25 ppb higher during humid heat than dry heat days. These groups of days occur during similar times of the year, with dry heat days ($n = 410$ over 2003–2021) occurring during May–September and humid heat days ($n = 102$) during June–September

https://doi.org/10.5194/egusphere-2025-4874
Preprint. Discussion started: 15 October 2025

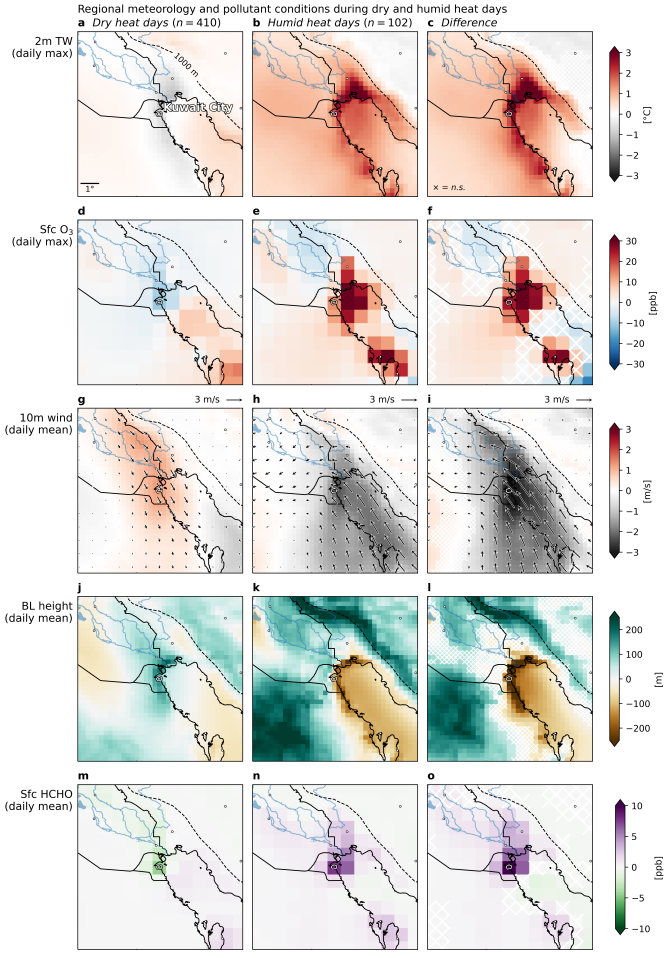

Figure 4. Regional meteorology and chemistry during dry and humid heat days in Kuwait City. a: Mean regional pattern of wet-bulb temperature anomalies during dry heat days in Kuwait City (n = 410 days over 2003–2021). The white contour outlines the city, smaller cities are shown as smaller dots, and a smoothed 1,000 meter elevation contour is shown. **b:** Same as **a** but for humid heat days (n = 102 days). **c:** Difference between humid and dry heat day composites (**b** minus **a**); white x's denote grid cells where differences are non-significant according to a bootstrapping procedure (see Data and Methods). **d–o:** Same as **a–c** but for O_3 anomalies (**d–f**), 10-meter wind speed anomalies (**g–i**, with wind direction anomalies overlaid as vectors), boundary layer height (**j–l**), and formaldehyde (HCHO; **m–o**). Meteorological variables are from ERA5 (wet-bulb temperature, wind, and boundary layer height), while chemical variables are from CAMSRA (O_3 and HCHO).

(Figure S8). Meteorologically, during dry heat days TW anomalies are slightly negative over the city, and on humid heat days positive TW anomalies are seen very concentrated along nearby Gulf coastline, maximizing at the mouth of the Tigris and Euphrates rivers; TW anomalies locally increase by ~ 2 °C at the Kuwait City gridcell. The extreme humid heat is colocated with stagnant near-surface conditions, with anomalously low wind speed and suppressed BL height displaying very similar

https://doi.org/10.5194/egusphere-2025-4874
Preprint. Discussion started: 15 October 2025

patterns to TW anomalies (and opposite conditions during dry heat days). Wind anomalies are northwesterly during dry heat days and southeasterly during humid heat days. Finally, during dry heat days HCHO concentration anomalies are negative in the center of the region but become positive during humid heat days, and their regional pattern is highly correlated with O_3. A similar signal is seen for NO_2 (Figure S8), implying that increases in both precursors are associated with stronger O_3 production—marine air over the northern Persian Gulf was shown to have high OH reactivity to both VOCs and NO_x due to intensive pollution from transport and oil and gas production, resulting in conditions very favorable for ozone production (Pfannerstill et al., 2019). Overall, meteorologically, dry heat days are associated with strong Shamal winds bringing hot, dry air from the northwest, whereas when these winds slacken and/or reverse, humidity can increase near the warm Gulf waters and TW can become extreme (Ivanovich et al., 2022; Raymond et al., 2021). We hypothesize that the stagnation involved in generating extreme TW, associated with reduced vertical mixing and horizontal outflow and suppressed boundary layer height, may simultaneously allow O_3 precursor species to become concentrated near the surface and O_3 production to increase.

In Figure 5, we similarly examine the regional meteorological and chemical processes leading to humid heat and $PM_{2.5}$ pollution co-occurrence in Shanghai, a prominent global hotspot (Figure 2c). We find again that the transition from dry to humid heat days in Shanghai corresponds with increased TW anomalies (though positive during both dry and humid heat days), decreased 10 m wind speeds (from positive to negative anomalies), and decreased boundary layer heights (from positive to negative anomalies) all colocated centering on the city, with winds becoming slightly less strongly offshore at the local city scale (regionally, wind direction differences are directed onshore from the north and offshore to the south). These days are again occupying the same season, both spanning from May to September ($n = 174$ dry heat days and $n = 364$ humid heat days). $PM_{2.5}$ anomalies surrounding Shanghai are negative during dry heat days and positive during humid heat days, with their regional difference patterns resembling those of both the meteorological conditions as well as HCHO (although HCHO is slightly positive during dry heat days as well). Hence, again, the distinct local meteorological drivers of extreme humid heat events in Shanghai also favor the local accumulation of—or the production of, through their influence on precursor species concentrations—$PM_{2.5}$ pollution.

3.4 Meteorological and chemical conditions associated with co-occurrence across global land area

We next investigate to what extent the drivers of extreme humid heat and air pollution co-occurrence found for the two previously-examined hotspots are generalizable to other global hotspots, or across global land area. Repeating composite analyses as in Figures 4 and 5 for the remaining hotspot regions (Figures S10–S16), we find that all regions show increased stagnation and nearly all show increased precursor concentrations on humid versus dry heat days, with spatially co-locating patterns—showing remarkable consistency between distinct hotspots. Moreover, in Figure 6a,c we quantify the correlations of O_3 and $PM_{2.5}$ concentrations against selected meteorological and compositional conditions, at the central gridcell of each hotspot region, and we find that largely similar roles of pollutant drivers are found across the hotspots. The correlations shown in Figure 6a,c are calculated across all extreme heat days (both dry and humid), in order to assess the underlying importance of the driver variables to pollution levels, before assessing how they differ between dry and humid heat days (Figure 6b,d). On average across all hotspot locations, O_3 and $PM_{2.5}$ are most highly correlated day-to-day with HCHO (at roughly $r = 0.75$ for O_3,

https://doi.org/10.5194/egusphere-2025-4874
Preprint. Discussion started: 15 October 2025

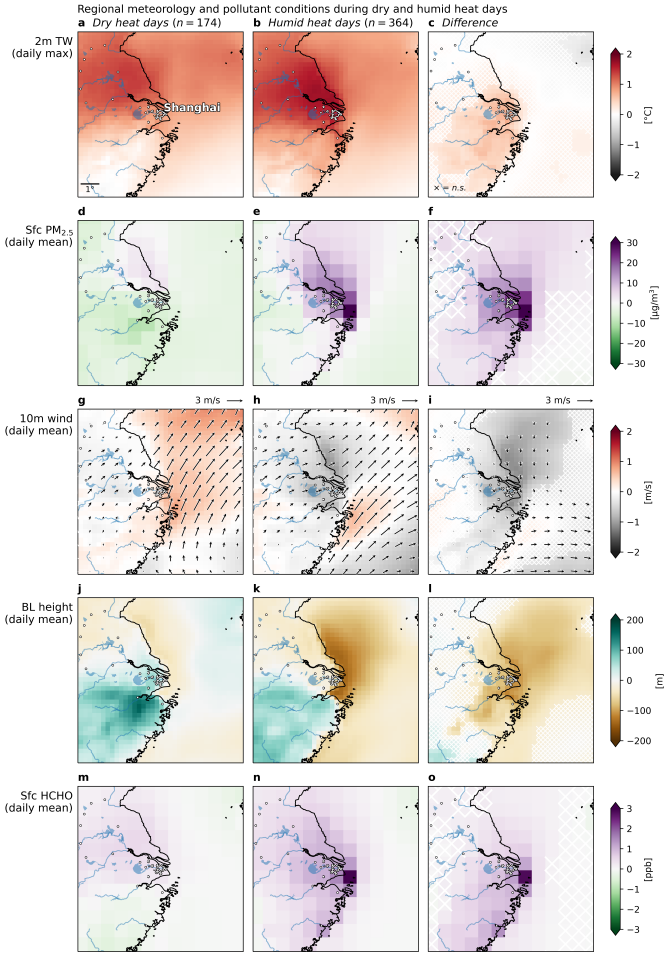

Figure 5. Regional meteorology and chemistry during dry and humid heat days in Shanghai. Same as Figure 4 but for dry and humid heat days in Shanghai (n = 174 and 364 respectively over 2003–2021), and with **d–f** displaying $PM_{2.5}$ instead of O_3 anomalies.

and roughly $r = 0.4$ for $PM_{2.5}$), followed closely by NO_2. For O_3, this may imply that these gridcells occupy NO_x-saturated or transitional regimes (as correlations with HCHO exceed those with NO_2 but both remain positive), consistent with Figure 3's demonstration that high co-occurrence values correspond with higher (but close to unity) background $\frac{NO_2}{HCHO}$ ratios. The purely-meteorological factors that O_3 and $PM_{2.5}$ are both most strongly correlated with are measures of near-surface stagnation: suppressed boundary layer height and low wind speed. The next most strongly-correlated variable is dewpoint temperature (measuring absolute, as opposed to relative, humidity of the air), which is positively correlated with both O_3 and $PM_{2.5}$. For $PM_{2.5}$ these correlations are nearly as strong as those with NO_2 and HCHO, implying a stronger role of meteorology in driving pollutant levels—as expected, given a smaller role of chemical production from precursors for $PM_{2.5}$ than O_3. Lastly, a small role is found for temperature, which is slightly positive for O_3 and near-zero for $PM_{2.5}$; this establishes interestingly

https://doi.org/10.5194/egusphere-2025-4874
Preprint. Discussion started: 15 October 2025

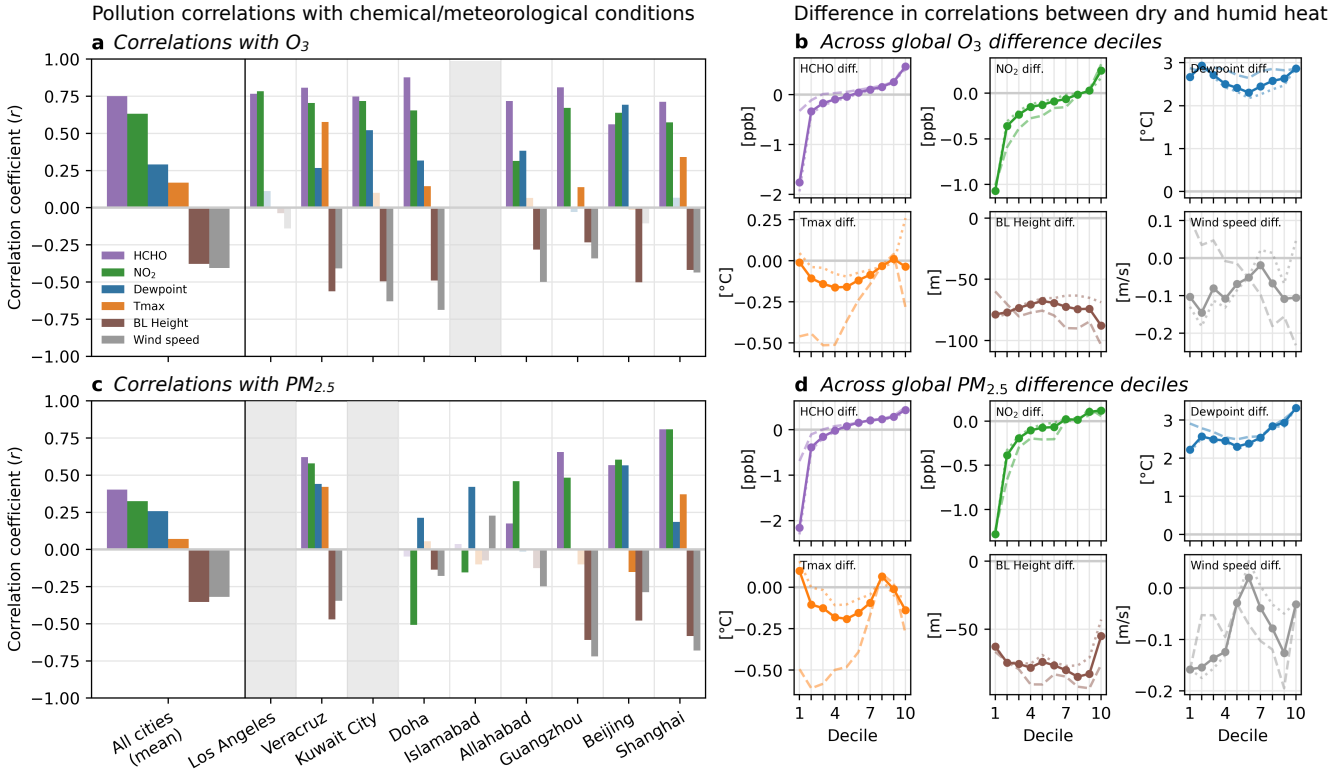

Figure 6. Contributions of meteorological and chemical drivers to humid heat and pollution co-occurrence. a: *Left panel:* Correlations between six individual chemical and meteorological variable anomalies (colored bars) and O_3 anomalies, across all heat days (both dry and humid) in the central city of each hotspot shown in Figure 2**a**, averaged across cities. For example, O_3 anomalies are correlated with HCHO anomalies at r = 0.75 on average across hotspot cities during extreme heat conditions. Meteorological variables on ERA5's high-resolution grid are averaged within the CAMSRA grid cell corresponding to each hotspot city. *Right panel:* Correlations for each hotspot city individually, with non-significant correlations in grayed colors. **b:** Placing hotspots within a global context, solid lines and markers show differences in six driver variable anomalies between humid and dry heat days averaged within each decile of O_3 and humid heat co-occurrence (values in Figure 2**a**). For example (*top left panel*), where O_3 and humid heat co-occurrence is strongest (high deciles), HCHO anomalies are higher during humid than during dry heat (and the opposite at low deciles). Dashed lines show areas with warm-season mean NO_2/HCHO ratio greater than unity; dotted lines show areas with ratio less than unity. **c–d:** Same as **a–b** but for $PM_{2.5}$. In **a**,**c**, regions that are not hotspots of each pollutant are masked with gray.

a more positive association of O_3 with humidity than with temperature. Fair consistency across individual hotspots in these relationships and their relative roles is also shown in Figure 6a,c, especially for O_3. For $PM_{2.5}$, notably, in some areas (Doha and Islamabad) its correlation with NO_2 is opposite to the behavior of other hotspots, and instead humidity is the dominant driver.

https://doi.org/10.5194/egusphere-2025-4874
Preprint. Discussion started: 15 October 2025

However, these correlations at hotspot gridcells do not necessarily indicate relationships unique to hotspot areas—hence, Figure 6b,d investigate (1) whether the conditions identified in Figure 6a,c as conducive to pollution are different between humid and dry heat days more generally across global land area, and (2) whether their difference is related to the strength of co-occurrence of humid heat and pollution. For example, while Figure 6a,c identify that O_3 and $PM_{2.5}$ are generally driven by HCHO and NO_2 during extreme heat days in co-occurrence hotspots, Figure 6b,d show that (1) in hotspot regions (high deciles on the x-axes) HCHO and NO_2 levels are higher during humid heat days than dry heat days, and (2) this difference is specific to strong hotspot regions, while areas occupying lower deciles of co-occurrence see strikingly opposite behavior. This implies that an underlying correlation of both HCHO and NO_2 with moisture during heat days, which only occurs in some regions, may be a significant factor determining the global hotspots of humid heat and pollution co-occurrence (as expected, this factor is more specific for O_3 than $PM_{2.5}$). In contrast, while in the highest deciles of co-occurrence humid heat is associated with high dewpoint, low boundary layer height, low wind speed anomalies, and minimal temperature anomaly signal (which are all consistent with Figure 6a,c), this is fairly unchanged across nearly all deciles of co-occurrence. However, when subsetting for areas occupying generally favorable background composition regimes—gridpoints with background $\frac{NO_2}{HCHO}$ ratios greater than unity (Figure 3)—stronger boundary layer height and wind speed differences are more specific to high co-occurrence deciles, for O_3 (dashed lines in Figure 6b). Additionally, for $PM_{2.5}$, stronger humidity differences are associated with stronger co-occurrence. Therefore, we hypothesize that for O_3, if given a more NO_x-saturated background composition, a stronger underlying association of humid heat with stagnant conditions (suppressed boundary layer height and slower wind speed) may help explain higher co-occurrence values in hotspot areas. For $PM_{2.5}$, we hypothesize that given a conducive background composition regime, a stronger humidity difference between humid and dry heat may be the most important factor, with wind speed and boundary layer height differences potentially contributing as well.

3.5 Multiple linear regression analysis of meteorological and chemical predictors of co-occurrence

We next test these hypotheses by investigating how strongly each of the six variables in Figure 6 (and their dependence on background chemistry regime) can explain the observed geographical patterns of co-occurrence. To quantify the relationship between co-occurrence and the six predictor variables within a single formula we construct a multiple linear regression model for O_3 and $PM_{2.5}$ respectively (Figure S17). For each pollutant, its respective mean co-occurrence with humid heat (i.e., values in Figure 2a,c) is taken as the dependent variable, and is formulated as a linear combination of the six anomaly differences (mean conditions on humid minus dry heat days), along with their interaction with background $\frac{NO_2}{HCHO}$, plus an intercept. Altogether, these variable anomaly differences as formulated in Figure 6 can explain 40% (spatial $r = 0.63$) of the geographical variation in O_3 anomaly difference, and 70% (spatial $r = 0.84$) of that of $PM_{2.5}$. As expected, for both pollutants, the precursor chemicals are the strongest predictors of increased pollution during humid heat, with HCHO most strongly predictive for both. In line with the hypotheses presented above, for O_3, the interaction terms of boundary layer height and wind speed with background $\frac{NO_2}{HCHO}$ are negative (i.e., with increasing $\frac{NO_2}{HCHO}$, the relationship between those variables and co-occurrence becomes more negative), confirming that given a higher $\frac{NO_2}{HCHO}$ ratio, the strength of stagnation during humid (versus dry) heat is predictive of higher O_3 concentrations during humid (versus dry) heat in a certain gridcell. Additionally, the coefficients

https://doi.org/10.5194/egusphere-2025-4874
Preprint. Discussion started: 15 October 2025

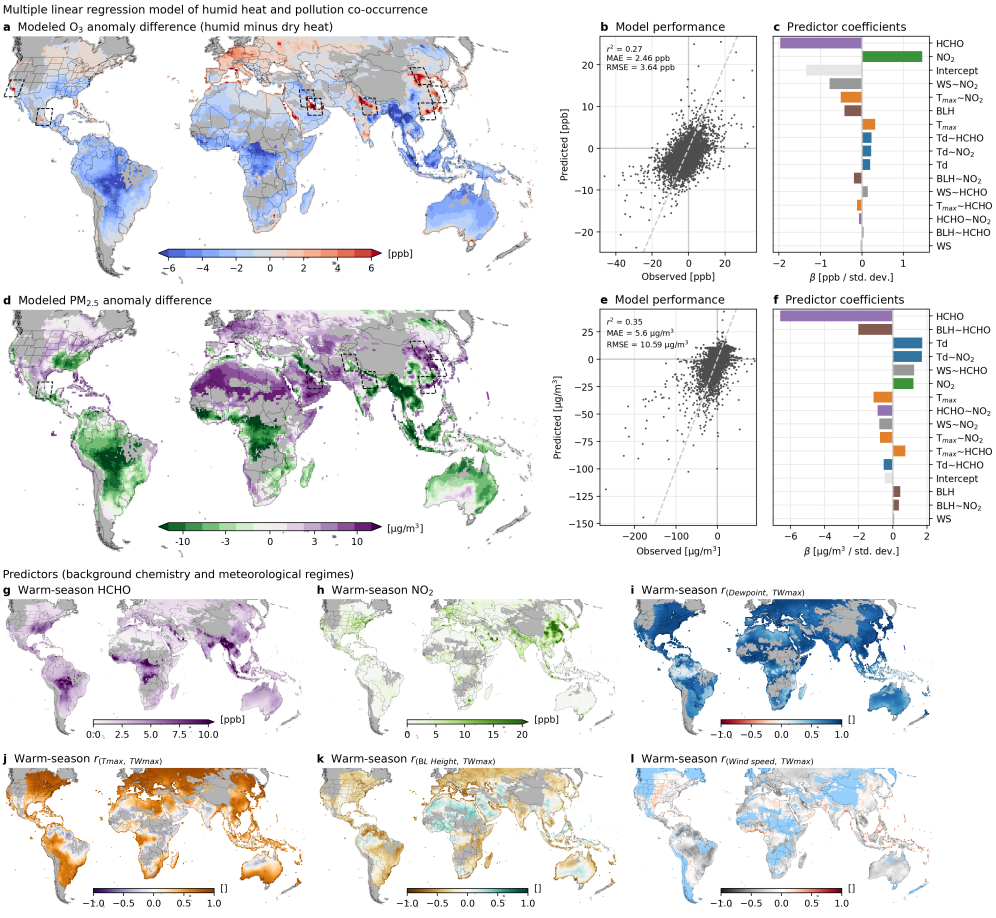

Figure 7. Multiple linear regression model of humid heat and pollution co-occurrence from simple background meteorological and chemical characteristics. a: O_3 anomaly difference between humid and dry heat days as predicted from intentionally-simple background factors. As in Figure 2**a**, but as predicted from the spatial patterns of six meteorological and chemical variables, which measure the background mix of related species and how strongly humid heat is associated with high temperatures, high humidity, or stagnation (specifically: warm-season mean concentrations of (1) HCHO and (2) NO_2, and warm-season daily correlations of wet-bulb temperature with (3) temperature, (4) dewpoint, (5) boundary layer height, and (6) wind speed). Interactions between meteorological factors and background precursor levels, as well as between the individual precursors, are also considered. **b:** Predicted humid minus dry heat differences in O_3 anomalies are plotted against observed differences; summary statistics of bias and explained variance and a line of equal observed and predicted values are shown. **c:** Linear regression coefficients for each predictor variable (and the intercept) are plotted from largest to smallest magnitude. Meteorological variable symbols (T_{max}, Td, BLH, and WS) represent the warm-season daily correlations of each with wet-bulb temperature, as described above. Tildes represent an interaction term between the left side and right side predictors; for example, the regression coefficient for the correlation of wind speed with wet-bulb temperature overall is near-zero (WS ≈ 0), but becomes negative with increasing background NO_2 (WS$\sim$NO$_2$ < 0) or decreasing HCHO (WS$\sim$HCHO > 0). Coefficients are standardized, representing the ppb of O_3 difference attributable to one standard deviation (calculated across non-excluded land area) variation in each predictor variable. **d–f:** As in **a–c** but for $PM_{2.5}$. **g–l:** Spatial patterns of each of the six predictor variables (in **l**, excluded land areas are shown in blue instead of gray).

https://doi.org/10.5194/egusphere-2025-4874
Preprint. Discussion started: 15 October 2025

for dewpoint and its interaction with $\frac{NO_2}{HCHO}$ are positive and T_{max}'s interaction with $\frac{NO_2}{HCHO}$ is negative, while the coefficients for T_{max}, boundary layer height, and wind speed by themselves are insignificant. For $PM_{2.5}$, also in line with the above hypotheses, increased moisture during humid heat is the strongest meteorological predictor of co-occurrence (by itself, while its interaction with $\frac{NO_2}{HCHO}$ is also positive). Additionally, wind speed and boundary layer height are found to be weakly positively predictive of co-occurrence, while T_{max} is nearly uncorrelated. These are mostly in line with Figure 6 with (differences in) T_{max} showing little trend and wind speed becoming more positive across deciles, although boundary layer height largely modestly decreases across deciles.

However, to more fundamentally explain why co-occurrence hotspot regions occur where they do, we ask: how much of the spatial variation in co-occurrence strength is explainable from *just* underlying meteorological and chemical regimes? In other words, we wish to test the role of purely background characteristics, which do not specifically index differences between dry and humid heat days, in determining whether areas experience strong co-occurrence (Figure 7). As above, for O_3 and $PM_{2.5}$ individually we construct a multiple linear regression model for the strength of their respective co-occurrence with humid heat. Again, six meteorological and compositional factors are included as explanatory variables, but here describing background characteristics: (1) warm-season HCHO levels, (2) warm-season NO_2 levels, and daily warm-season correlation of TW_{max} with (3) dewpoint, (4) T_{max}, (5) boundary layer height, and (6) wind speed (warm season as defined above). We also allow interaction terms between the four meteorological factors and each of the compositional factors, as well as between the two precursors.

We find that these intentionally simple background meteorological and compositional factors still together explain a substantial part of the observed geographical variability in co-occurrence strength. Overall, the model explains 27% of the observed variability for O_3 co-occurrence (spatial correlation of $r = 0.52$; $r^2 = 0.27$) and 35% for $PM_{2.5}$ ($r = 0.59$; $r^2 = 0.35$)—representing large fractions of the 40% and 70% (respectively) explained by the model based on the actual conditions during humid versus dry heat. For O_3, background chemistry regime is the most predictive factor: low HCHO and high NO_2 in the warm season are conducive for stronger co-occurrence, as previously found (Figure 3), with modeled increases of nearly 2 and 1.5 ppb O_3 (of difference between humid and dry heat days) per standard deviation decrease of HCHO and increase of NO_2, respectively. Meteorological factors are in line with the hypotheses above: more negative boundary layer height–TW_{max} correlations are predictive of co-occurrence, especially in higher-NO_2 areas; more negative wind speed–TW_{max} correlations are predictive of co-occurrence in higher-NO_2 (e.g., becoming the strongest non-compositional coefficient in places at one standard deviation above the mean of NO_2) and lower-HCHO areas, but not overall; and more positive dewpoint–TW_{max} correlations are predictive of co-occurrence overall and especially in higher-NO_2 areas, but also in higher-HCHO areas (implying some cancellation). Additionally, more positive T_{max}–TW_{max} correlations are predictive of co-occurrence overall but less so with increasing NO_2 (beginning to reverse at about a half standard deviation above the mean of NO_2). For $PM_{2.5}$, low background HCHO is the most important predictor of co-occurrence, with a modeled increase of over 6 $\mu g/m^3$ $PM_{2.5}$ per standard deviation decrease of HCHO; high NO_2 is also predictive but more weakly than some meteorological factors. As hypothesized, more positive dewpoint–TW_{max} correlation is the most predictive meteorological factor main effect (coefficient of nearly 2 $\mu g/m^3$ per standard deviation), with its coefficient almost doubling per standard deviation NO_2 increase and reducing with increasing

https://doi.org/10.5194/egusphere-2025-4874
Preprint. Discussion started: 15 October 2025

HCHO. Here, the role of stagnation conditions is conflicted, with more negative wind speed–TW_{max} correlation predictive of co-occurrence under favorable background composition (higher NO_2 and lower HCHO) but boundary layer height–TW_{max} correlation weakly positively predictive overall, and increasingly so at more favorable (lower) HCHO levels. Finally, negative T_{max}–TW_{max} correlations are predictive of co-occurrence, and more so with favorable background composition.

Additionally, we note that even with this linear combination of simple background meteorological and chemical characteristics, co-occurrence hotspotting behavior is observed, with nearly all of the observed hotspots of co-occurrence reproduced (Figure 7a,d), implying that the mechanisms driving co-occurrence are roughly consistent between hotspots and the rest of the land area. However, as hotspots are by definition far from the bulk of the co-occurrence value distribution, the model typically underestimates the magnitude of their co-occurrence values (as well as that of negative extremes). Additionally, some specific hotspots seen in CAMSRA data are not well reproduced by the model: the Veracruz hotspot is only slightly reproduced for both O_3 and $PM_{2.5}$, and the Islamabad hotspot for $PM_{2.5}$ is simulated in the opposite direction. Note that in Figure 6, $PM_{2.5}$'s correlations with driver variables at the Islamabad gridcell are not representative of other hotspot areas, with NO_2 being negatively correlated and stagnation variables uncorrelated, although humidity is still positively correlated; this implies that moisture advection, associated with changing wind direction rather than reduced wind speed, may play a dominant role. This is true of Doha as well (Figure 6), and it is evident that the gridcells on the Qatar peninsula are also simulated in the wrong direction, but in the directly-surrounding region a hotspot is still reproduced. We hypothesize that in these areas, $PM_{2.5}$ and humid heat co-occurrence are driven by mechanisms different from most other gridcells, so the single regression formula fit to all gridcells is less appropriate.

In summary, our multiple linear regression analysis provides quantitative evidence that global hotspots of humid heat and pollution co-occurrence arise in substantial part from background compositional and meteorological regimes. It most robustly shows that (1) O_3 and $PM_{2.5}$ co-occurrence with extreme humid heat is highly determined by background local compositional regimes, with O_3 co-occurrence spatially associated with high NO_2 and low HCHO, and $PM_{2.5}$ co-occurrence mostly associated with low HCHO; (2) for O_3, especially where the background composition is favorable (i.e., high NO_2 and low HCHO), co-occurrence is driven by an underlying meteorological regime of more stagnant conditions on higher-TW_{max} days; and (3) for $PM_{2.5}$, co-occurrence is directly driven by increased humidity during higher-TW_{max} days, and thus is typically stronger in places where TW_{max} is more strongly correlated with dewpoint. These findings are in line with the quantile-based approach in Figure 6, which also shows that higher HCHO and NO_2 concentrations during humid versus dry heat are associated with stronger co-occurrence. Our analysis raises the question of why a lower-HCHO and higher-NO_2 background composition should be favorable for co-occurrence behavior, and we hypothesize further in Conclusions and Discussion.

4 Conclusions and Discussion

The main conclusions of this study can be summarized as follows:

1. We identify regions worldwide where O_3 and/or $PM_{2.5}$ pollution tend to be higher during extreme humid heat than extreme dry heat—i.e., where increased heat stress tends to co-occur with increased pollution, revealing a preferential tem-

https://doi.org/10.5194/egusphere-2025-4874
Preprint. Discussion started: 15 October 2025

poral compounding, rather than compensation, of hazards. We investigate the mechanistic drivers of this co-occurrence of hazards, on local to global scales.

2. Such regions include several of the globally most-extreme humid heat hotspots, and many densely-populated areas, emphasizing their potential human health relevance: altogether, a greater population is exposed to worsened than alleviated pollution during humid heat.

3. Regions that experience stronger co-occurrence of humid heat and pollution tend to occupy more urban atmospheric composition regimes, with typically higher NO_x and lower VOC concentrations. This association is stronger for O_3 than for $PM_{2.5}$.

4. Among regions with favorable (higher-$\frac{NO_2}{HCHO}$) background chemistry regimes, co-occurrence of extreme humid heat and air pollution generally arises in places where the typical meteorological drivers of extreme humid heat (which can vary widely) are also conducive to the build-up of pollutants and/or their precursors. For O_3, co-occurrence is stronger where humid heat is more strongly associated with atmospheric stagnation (low boundary layer height and weak winds), and this relationship strengthens where background NO_2 is higher and HCHO is lower. For $PM_{2.5}$, co-occurrence is stronger where humid heat is more strongly driven by higher humidity rather than stagnation, suggesting that advection and a direct contribution of hygroscopic growth may be more relevant drivers than for O_3.

5. This work corroborates a prior regional investigation showing co-occurrence between humid heat and both O_3 and $PM_{2.5}$ in Beijing and emphasizing the importance of boundary layer behavior (Miao et al., 2022), but expands to a global scope and shows that many of the locally-relevant mechanisms are also relevant in many other hotspots of co-occurrence.

The primary implication of our work is that in many locations worldwide, moist heat stress and air pollution tend to be worse at the same times, and that this tendency, heretofore unstudied at a global scale, affects a large proportion of the world's population. We discuss additional speculative implications and questions below.

One question raised by our analysis is why many hotspots of humid heat and air pollution co-occurrence are also global hotspots of extreme humid heat. Is there something specific about the climatological or meteorological conditions enabling the most extreme humid heat worldwide that is also conducive to pollution enhancement? Raymond et al. (2021) showed that globally-extreme humid heat occurs in locations where near-surface moist enthalpy can accumulate to extreme levels without convection being triggered to discharge it; this combination requires a climatologically-hot location that is associated with both a plentiful moisture source (e.g., a moist land surface or proximal body of warm water) and some mechanism of suppression of convection. Duan et al. (2024) found that dry air in the lower free troposphere plays a key role in enabling the most extreme humid heat via convective inhibition. This confluence of factors is most favored in the subtropics, whereas within the tropics, by contrast, extreme humid heat hotspots are less sustainable because the atmosphere is more chronically unstable and free-tropospheric temperature, which acts as a top-down control on convection, is constrained to be more spatially uniform (Zhang et al., 2021). We propose that the convective inhibition enabling extreme humid heat events also contributes to the accumulation of pollution in the boundary layer (as supported by our results highlighting the role of stagnation), and that the fact that this

https://doi.org/10.5194/egusphere-2025-4874
Preprint. Discussion started: 15 October 2025

mechanism is common among globally-extreme humid heat hotspots accounts in some part for their geographical overlapping with the hotspots we identify here, where humid heat is accompanied by higher air pollution.

Additionally, our finding that the co-occurrence of humid heat and air pollution is more likely in regions with higher NO_2 and lower HCHO levels raises the question of why a more urban, NO_x-saturated background chemistry regime should be predictive of higher co-occurrence—i.e., whether this type of background chemistry helps mechanistically drive co-occurrence or is simply correlated with it. Consulting the spatial distributions of NO_2 and HCHO (Figure 7g–h) we note that there is a clear correspondence of tropical high-HCHO regions—in central South America, central Africa flanking the equator, and southeast Asia—with negative pollution co-occurrence in the same areas (Figure 2a,c). This pattern represents high HCHO emissions from tropical forests (dry or moist, but not rainforests), which are known to dominantly contribute to the global HCHO budget (Guenther et al., 1995, 2006). Biogenic emissions of VOCs, including HCHO and isoprene, are highly sensitive to heat and drought, increasing nonlinearly in temperature and enhanced under dry conditions (Guenther et al., 1993; Porter and Heald, 2019; Duncan et al., 2009; Naimark et al., 2021; Zheng et al., 2017; Strada et al., 2023). Correspondingly, we find strong anomalies of both O_3 and $PM_{2.5}$ during dry heat days in all of these tropical (non-rainforest) forest areas (Figure 1a,b), which disappear during humid heat days, thus driving the negative co-occurrence seen in Figure 2a,c. Increased wildfire activity could additionally lead to higher ozone and particulate pollution during dry heat in these areas. In contrast, many hotspots of humid heat and pollution co-occurrence arise in areas with high NO_2—these areas are typically not devoid of HCHO (Figure 7g) but since they are more urban their VOC mixture is likely more anthropogenic in origin (Li et al., 2024). We hypothesize that in these areas it is less the emission of precursors that is sensitive to environmental conditions but more their concentration in the boundary layer, leading to accumulation during humid heat events brought about by stagnant conditions. A higher background NO_2/HCHO ratio could therefore be predictive of high co-occurrence because it indicates a more anthropogenically-influenced chemical regime wherein a stronger mechanical trapping of pollutant precursors during humid heat conditions outweighs any increased biogenic emission of precursors during dry heat. As noted in Data and Methods, biogenic VOC emissions in CAMSRA, though calculated from hourly meteorological inputs by the MEGAN model, are at monthly temporal resolution (Inness et al., 2019; Sindelarova et al., 2014). Our daily-scale analysis therefore likely reflects the impacts of changes in meteorological conditions more than in emissions—hence in negative co-occurrence areas, while biogenic emissions likely still record the influence of daily-scale dry versus humid heat on a monthly timescale, meteorology likely also plays a role.

It is also possible that, in addition to its mechanical boundary-layer-associated effects, humid heat could play a direct chemical role increasing the production of ozone and/or $PM_{2.5}$. Regions of high co-occurrence, typically dry and NO_x-saturated areas, could be sensitive to the availability of water vapor as a source for HO_x radicals, and hence under HO_x-limited regimes of secondary ozone and $PM_{2.5}$ production. Assessing whether the makeup of $PM_{2.5}$ during humid heat favors secondary species could help determine whether increased pollution during humid heat is due more to chemical production versus boundary layer accumulation. Furthermore, identifying the importance of HO_x-limitation could help explain the dependence of co-occurrence strength on background chemical regime. Overall, further research should pursue a more targeted, process-based understanding of why a more anthropogenically-influenced chemistry regime is predictive of higher co-occurrence of extreme humid heat and air pollution.

https://doi.org/10.5194/egusphere-2025-4874
Preprint. Discussion started: 15 October 2025

Code and data availability. The CAMSRA and ERA5 reanalysis data used in this study are publicly available from ECMWF, downloadable at https://ads.atmosphere.copernicus.eu/datasets/cams-global-reanalysis-eac4?tab=download and https://cds.climate.copernicus.eu/datasets/reanalysis-era5-single-levels?tab=download, respectively. The AirNow data from U.S. Embassies used for comparison in the Supplementary Information has been removed and sharing has been halted (previously available at https://www.airnow.gov/international/us-embassies-and-consulates/), but is available from the authors on request. Code to produce the figures was written in Python in Jupyter Notebooks and is available from the authors on request.

Author contributions. STB, YW, MT, and AF designed the study. STB performed the analysis with input from all authors, prepared the figures, and wrote the first draft of the manuscript. All authors discussed and edited the paper.

Competing interests. The authors declare no competing interests.

Acknowledgements. We are thankful to Cheng Zheng for valuable input early in this project and to Radley Horton for helpful discussions throughout. STB was supported by the NASA FINESST fellowship program (award number 80NSSC22K1444).

https://doi.org/10.5194/egusphere-2025-4874
Preprint. Discussion started: 15 October 2025

References

Ali, M. A., Bilal, M., Wang, Y., Nichol, J. E., Mhawish, A., Qiu, Z., de Leeuw, G., Zhang, Y., Zhan, Y., Liao, K., Almazroui, M., Dambul, R., Shahid, S., and Islam, M. N.: Accuracy assessment of CAMS and MERRA-2 reanalysis PM2.5 and PM10 concentrations over China, Atmospheric Environment, 288, 119 297, https://doi.org/10.1016/j.atmosenv.2022.119297, 2022.

Anenberg, S. C., Haines, S., Wang, E., Nassikas, N., and Kinney, P. L.: Synergistic health effects of air pollution, temperature, and pollen exposure: a systematic review of epidemiological evidence, Environmental Health, 19, 130, https://doi.org/10.1186/s12940-020-00681-z, 2020.

Ballester, J., Quijal-Zamorano, M., Méndez Turrubiates, R. F., Pegenaute, F., Herrmann, F. R., Robine, J. M., Basagaña, X., Tonne, C., Antó, J. M., and Achebak, H.: Heat-related mortality in Europe during the summer of 2022, Nature Medicine, 29, 1857–1866, https://doi.org/10.1038/s41591-023-02419-z, publisher: Nature Publishing Group, 2023.

Barriopedro, D., García-Herrera, R., Ordóñez, C., Miralles, D., and Salcedo-Sanz, S.: Heat waves: Physical understanding and scientific challenges, Reviews of Geophysics, 61, e2022RG000 780, 2023.

Basu, R. and Samet, J. M.: Relation between Elevated Ambient Temperature and Mortality: A Review of the Epidemiologic Evidence, Epidemiologic Reviews, 24, 190–202, https://doi.org/10.1093/epirev/mxf007, 2002.

Camalier, L., Cox, W., and Dolwick, P.: The effects of meteorology on ozone in urban areas and their use in assessing ozone trends, Atmospheric Environment, 41, 7127–7137, https://doi.org/10.1016/j.atmosenv.2007.04.061, 2007.

Cheng, Y., He, K.-b., Du, Z.-y., Zheng, M., Duan, F.-k., and Ma, Y.-l.: Humidity plays an important role in the PM2. 5 pollution in Beijing, Environmental pollution, 197, 68–75, 2015.

Cohen, A. J., Ross Anderson, H., Ostro, B., Pandey, K. D., Krzyzanowski, M., Künzli, N., Gutschmidt, K., Pope, A., Romieu, I., Samet, J. M., and Smith, K.: The global burden of disease due to outdoor air pollution, Journal of Toxicology and Environmental Health. Part A, 68, 1301–1307, https://doi.org/10.1080/15287390590936166, 2005.

Dawson, J. P., Bloomer, B. J., Winner, D. A., and Weaver, C. P.: Understanding the Meteorological Drivers of U.S. Particulate Matter Concentrations in a Changing Climate, https://doi.org/10.1175/BAMS-D-12-00181.1, section: Bulletin of the American Meteorological Society, 2014.

Duan, S. Q., Ahmed, F., and Neelin, J. D.: Moist heatwaves intensified by entrainment of dry air that limits deep convection, Nature Geoscience, 17, 837–844, 2024.

Duncan, B. N., Yoshida, Y., Damon, M. R., Douglass, A. R., and Witte, J. C.: Temperature dependence of factors controlling isoprene emissions, Geophysical Research Letters, 36, 2009.

Fiore, A. M., Naik, V., Spracklen, D. V., Steiner, A., Unger, N., Prather, M., Bergmann, D., Cameron-Smith, P. J., Cionni, I., Collins, W. J., Dalsøren, S., Eyring, V., Folberth, G. A., Ginoux, P., Horowitz, L. W., Josse, B., Lamarque, J.-F., MacKenzie, I. A., Nagashima, T., O'Connor, F. M., Righi, M., Rumbold, S. T., Shindell, D. T., Skeie, R. B., Sudo, K., Szopa, S., Takemura, T., and Zeng, G.: Global air quality and climate, Chemical Society Reviews, 41, 6663–6683, https://doi.org/10.1039/C2CS35095E, publisher: The Royal Society of Chemistry, 2012.

Fiore, A. M., , Vaishali, N., , and Leibensperger, E. M.: Air Quality and Climate Connections, Journal of the Air & Waste Management Association, 65, 645–685, https://doi.org/10.1080/10962247.2015.1040526, publisher: Taylor & Francis, 2015.

Flemming, J., Huijnen, V., Arteta, J., Bechtold, P., Beljaars, A., Blechschmidt, A.-M., Diamantakis, M., Engelen, R. J., Gaudel, A., Inness, A., Jones, L., Josse, B., Katragkou, E., Marecal, V., Peuch, V.-H., Richter, A., Schultz, M. G., Stein, O., and Tsikerdekis, A.: Tropospheric

https://doi.org/10.5194/egusphere-2025-4874
Preprint. Discussion started: 15 October 2025

chemistry in the Integrated Forecasting System of ECMWF, Geoscientific Model Development, 8, 975–1003, https://doi.org/10.5194/gmd-8-975-2015, publisher: Copernicus GmbH, 2015.

Fu, T.-M. and Tian, H.: Climate Change Penalty to Ozone Air Quality: Review of Current Understandings and Knowledge Gaps, Current Pollution Reports, 5, 159–171, https://doi.org/10.1007/s40726-019-00115-6, 2019.

Gasparrini, A., Guo, Y., Hashizume, M., Lavigne, E., Zanobetti, A., Schwartz, J., Tobias, A., Tong, S., Rocklöv, J., Forsberg, B., Leone, M., Sario, M. D., Bell, M. L., Guo, Y.-L. L., Wu, C.-f., Kan, H., Yi, S.-M., Coelho, M. d. S. Z. S., Saldiva, P. H. N., Honda, Y., Kim, H., and Armstrong, B.: Mortality risk attributable to high and low ambient temperature: a multicountry observational study, The Lancet, 386, 369–375, https://doi.org/10.1016/S0140-6736(14)62114-0, publisher: Elsevier, 2015.

Gopikrishnan, G. S., Westervelt, D. M., and Kuttippurath, J.: Aerosol inhibition on photochemical surface ozone formation under future climate and air quality scenarios, npj Climate and Atmospheric Science, 8, 154, https://doi.org/10.1038/s41612-025-01048-2, publisher: Nature Publishing Group, 2025.

Granier, C., Bessagnet, B., Bond, T., D'Angiola, A., Denier van der Gon, H., Frost, G. J., Heil, A., Kaiser, J. W., Kinne, S., Klimont, Z., Kloster, S., Lamarque, J.-F., Liousse, C., Masui, T., Meleux, F., Mieville, A., Ohara, T., Raut, J.-C., Riahi, K., Schultz, M. G., Smith, S. J., Thompson, A., van Aardenne, J., van der Werf, G. R., and van Vuuren, D. P.: Evolution of anthropogenic and biomass burning emissions of air pollutants at global and regional scales during the 1980–2010 period, Climatic Change, 109, 163, https://doi.org/10.1007/s10584-011-0154-1, 2011.

Guenther, A., Hewitt, C. N., Erickson, D., Fall, R., Geron, C., Graedel, T., Harley, P., Klinger, L., Lerdau, M., McKay, W., et al.: A global model of natural volatile organic compound emissions, Journal of Geophysical Research: Atmospheres, 100, 8873–8892, 1995.

Guenther, A., Karl, T., Harley, P., Wiedinmyer, C., Palmer, P. I., and Geron, C.: Estimates of global terrestrial isoprene emissions using MEGAN (Model of Emissions of Gases and Aerosols from Nature), Atmospheric Chemistry and Physics, 6, 3181–3210, 2006.

Guenther, A. B., Zimmerman, P. R., Harley, P. C., Monson, R. K., and Fall, R.: Isoprene and monoterpene emission rate variability: model evaluations and sensitivity analyses, Journal of Geophysical Research: Atmospheres, 98, 12 609–12 617, 1993.

Haldane, J. S.: The Influence of High Air Temperatures No. I, Epidemiology & Infection, 5, 494–513, https://doi.org/10.1017/S0022172400006811, 1905.

Hersbach, H., Bell, B., Berrisford, P., Hirahara, S., Horányi, A., Muñoz-Sabater, J., Nicolas, J., Peubey, C., Radu, R., Schepers, D., et al.: The ERA5 global reanalysis, Quarterly Journal of the Royal Meteorological Society, 146, 1999–2049, 2020.

Horton, R. M., Mankin, J. S., Lesk, C., Coffel, E., and Raymond, C.: A Review of Recent Advances in Research on Extreme Heat Events, Current Climate Change Reports, 2, 242–259, https://doi.org/10.1007/s40641-016-0042-x, 2016.

Huang, C., Barnett, A. G., Wang, X., Vaneckova, P., FitzGerald, G., and Tong, S.: Projecting Future Heat-Related Mortality under Climate Change Scenarios: A Systematic Review, Environmental Health Perspectives, 119, 1681–1690, https://doi.org/10.1289/ehp.1103456, publisher: Environmental Health Perspectives, 2011.

Im, E.-S., Pal, J. S., and Eltahir, E. A. B.: Deadly heat waves projected in the densely populated agricultural regions of South Asia, Science Advances, 3, e1603 322, https://doi.org/10.1126/sciadv.1603322, publisher: American Association for the Advancement of Science Section: Research Article, 2017.

Inness, A., Ades, M., Agustí-Panareda, A., Barré, J., Benedictow, A., Blechschmidt, A.-M., Dominguez, J. J., Engelen, R., Eskes, H., Flemming, J., et al.: The CAMS reanalysis of atmospheric composition, Atmospheric Chemistry and Physics, 19, 3515–3556, 2019.

Ivanovich, C., Anderson, W., Horton, R., Raymond, C., and Sobel, A.: The influence of intraseasonal oscillations on humid heat in the Persian Gulf and South Asia, Journal of Climate, 35, 4309–4329, 2022.

https://doi.org/10.5194/egusphere-2025-4874
Preprint. Discussion started: 15 October 2025

Jacob, D. J. and Winner, D. A.: Effect of climate change on air quality, Atmospheric Environment, 43, 51–63, https://doi.org/10.1016/j.atmosenv.2008.09.051, 2009.

Jacob, D. J., Logan, J. A., Gardner, G. M., Yevich, R. M., Spivakovsky, C. M., Wofsy, S. C., Sillman, S., and Prather, M. J.: Factors regulating ozone over the United States and its export to the global atmosphere, Journal of Geophysical Research: Atmospheres, 98, 14 817–14 826, https://doi.org/10.1029/98JD01224, _eprint: https://onlinelibrary.wiley.com/doi/pdf/10.1029/98JD01224, 1993.

Jin, C., Wang, Y., Li, T., and Yuan, Q.: Global validation and hybrid calibration of CAMS and MERRA-2 PM2.5 reanalysis products based on OpenAQ platform, Atmospheric Environment, 274, 118 972, https://doi.org/10.1016/j.atmosenv.2022.118972, 2022.

Kaiser, J. W., Heil, A., Andreae, M. O., Benedetti, A., Chubarova, N., Jones, L., Morcrette, J.-J., Razinger, M., Schultz, M. G., Suttie, M., and van der Werf, G. R.: Biomass burning emissions estimated with a global fire assimilation system based on observed fire radiative power, Biogeosciences, 9, 527–554, https://doi.org/10.5194/bg-9-527-2012, publisher: Copernicus GmbH, 2012.

Kavassalis, S. C. and Murphy, J. G.: Understanding ozone-meteorology correlations: A role for dry deposition, Geophysical Research Letters, 44, 2922–2931, https://doi.org/https://doi.org/10.1002/2016GL071791, _eprint: https://agupubs.onlinelibrary.wiley.com/doi/pdf/10.1002/2016GL071791, 2017.

Kerr, G. H., Waugh, D. W., Steenrod, S. D., Strode, S. A., and Strahan, S. E.: Surface Ozone-Meteorology Relationships: Spatial Variations and the Role of the Jet Stream, Journal of Geophysical Research: Atmospheres, 125, e2020JD032 735, https://doi.org/10.1029/2020JD032735, _eprint: https://onlinelibrary.wiley.com/doi/pdf/10.1029/2020JD032735, 2020.

Kumar, R., Barth, M. C., Pfister, G., Delle Monache, L., Lamarque, J., Archer-Nicholls, S., Tilmes, S., Ghude, S., Wiedinmyer, C., Naja, M., et al.: How will air quality change in South Asia by 2050?, Journal of Geophysical Research: Atmospheres, 123, 1840–1864, 2018.

Lacima, A., Petetin, H., Soret, A., Bowdalo, D., Jorba, O., Chen, Z., Méndez Turrubiates, R. F., Achebak, H., Ballester, J., and Pérez García-Pando, C.: Long-term evaluation of surface air pollution in CAMSRA and MERRA-2 global reanalyses over Europe (2003–2020), Geoscientific Model Development, 16, 2689–2718, https://doi.org/10.5194/gmd-16-2689-2023, publisher: Copernicus GmbH, 2023.

Lelieveld, J., Evans, J. S., Fnais, M., Giannadaki, D., and Pozzer, A.: The contribution of outdoor air pollution sources to premature mortality on a global scale, Nature, 525, 367–371, https://doi.org/10.1038/nature15371, publisher: Nature Publishing Group, 2015.

Lesk, C., Rowhani, P., and Ramankutty, N.: Influence of extreme weather disasters on global crop production, Nature, 529, 84–87, https://doi.org/10.1038/nature16467, publisher: Nature Publishing Group, 2016.

Li, C., van Donkelaar, A., Hammer, M. S., McDuffie, E. E., Burnett, R. T., Spadaro, J. V., Chatterjee, D., Cohen, A. J., Apte, J. S., Southerland, V. A., Anenberg, S. C., Brauer, M., and Martin, R. V.: Reversal of trends in global fine particulate matter air pollution, Nature Communications, 14, 5349, https://doi.org/10.1038/s41467-023-41086-z, publisher: Nature Publishing Group, 2023.

Li, K., Jacob, D. J., Liao, H., Zhu, J., Shah, V., Shen, L., Bates, K. H., Zhang, Q., and Zhai, S.: A two-pollutant strategy for improving ozone and particulate air quality in China, Nature Geoscience, 12, 906–910, https://doi.org/10.1038/s41561-019-0464-x, publisher: Nature Publishing Group, 2019.

Li, X., Zhu, L., De Smedt, I., Sun, W., Chen, Y., Shu, L., Wang, D., Liu, S., Pu, D., Li, J., et al.: Global temperature dependency of biogenic HCHO columns observed from space: Interpretation of TROPOMI results using GEOS-Chem model, Journal of Geophysical Research: Atmospheres, 129, e2024JD041 784, 2024.

Lu, X., Hong, J., Zhang, L., Cooper, O. R., Schultz, M. G., Xu, X., Wang, T., Gao, M., Zhao, Y., and Zhang, Y.: Severe Surface Ozone Pollution in China: A Global Perspective, Environmental Science & Technology Letters, 5, 487–494, https://doi.org/10.1021/acs.estlett.8b00366, publisher: American Chemical Society, 2018.

https://doi.org/10.5194/egusphere-2025-4874
Preprint. Discussion started: 15 October 2025

Matthews, T., Byrne, M., Horton, R., Murphy, C., Pielke Sr, R., Raymond, C., Thorne, P., and Wilby, R. L.: Latent heat must be visible in climate communications, WIREs Climate Change, 13, e779, https://doi.org/10.1002/wcc.779, _eprint: https://onlinelibrary.wiley.com/doi/pdf/10.1002/wcc.779, 2022.

Meehl, G. A. and Tebaldi, C.: More Intense, More Frequent, and Longer Lasting Heat Waves in the 21st Century, Science, https://www.science.org/doi/10.1126/science.1098704, 2004.

Miao, Y., Che, H., Liu, S., and Zhang, X.: Heat stress in Beijing and its relationship with boundary layer structure and air pollution, Atmospheric Environment, 282, 119 159, 2022.

Mora, C., Dousset, B., Caldwell, I. R., Powell, F. E., Geronimo, R. C., Bielecki, C. R., Counsell, C. W. W., Dietrich, B. S., Johnston, E. T., Louis, L. V., Lucas, M. P., McKenzie, M. M., Shea, A. G., Tseng, H., Giambelluca, T. W., Leon, L. R., Hawkins, E., and Trauernicht, C.: Global risk of deadly heat, Nature Climate Change, 7, 501–506, https://doi.org/10.1038/nclimate3322, publisher: Nature Publishing Group, 2017.

Naimark, J. G., Fiore, A. M., Jin, X., Wang, Y., Klovenski, E., and Braneon, C.: Evaluating drought responses of surface ozone precursor proxies: Variations with land cover type, precipitation, and temperature, Geophysical Research Letters, 48, e2020GL091 520, 2021.

Pal, J. S. and Eltahir, E. A. B.: Future temperature in southwest Asia projected to exceed a threshold for human adaptability, Nature Climate Change, 6, 197–200, https://doi.org/10.1038/nclimate2833, number: 2 Publisher: Nature Publishing Group, 2016.

Pfannerstill, E. Y., Wang, N., Edtbauer, A., Bourtsoukidis, E., Crowley, J. N., Dienhart, D., Eger, P. G., Ernle, L., Fischer, H., Hottmann, B., et al.: Shipborne measurements of total OH reactivity around the Arabian Peninsula and its role in ozone chemistry, Atmospheric Chemistry and Physics, 19, 11 501–11 523, 2019.

Pope III, C. A., Burnett, R. T., Thun, M. J., Calle, E. E., Krewski, D., Ito, K., and Thurston, G. D.: Lung Cancer, Cardiopulmonary Mortality, and Long-term Exposure to Fine Particulate Air Pollution, JAMA, 287, 1132–1141, https://doi.org/10.1001/jama.287.9.1132, 2002.

Porter, W. C. and Heald, C. L.: The mechanisms and meteorological drivers of the summertime ozone–temperature relationship, Atmospheric Chemistry and Physics, 19, 13 367–13 381, 2019.

Pozzer, A., Steffens, B., Proestos, Y., Sciare, J., Akritidis, D., Chowdhury, S., Burkart, K., and Bacer, S.: Atmospheric health burden across the century and the accelerating impact of temperature compared to pollution, Nature Communications, 15, 9379, https://doi.org/10.1038/s41467-024-53649-9, publisher: Nature Publishing Group, 2024.

Pye, H. O. T., Liao, H., Wu, S., Mickley, L. J., Jacob, D. J., Henze, D. K., and Seinfeld, J. H.: Effect of changes in climate and emissions on future sulfate-nitrate-ammonium aerosol levels in the United States, Journal of Geophysical Research: Atmospheres, 114, https://doi.org/10.1029/2008JD010701, _eprint: https://onlinelibrary.wiley.com/doi/pdf/10.1029/2008JD010701, 2009.

Rahman, M. M., McConnell, R., Schlaerth, H., Ko, J., Silva, S., Lurmann, F. W., Palinkas, L., Johnston, J., Hurlburt, M., Yin, H., Ban-Weiss, G., and Garcia, E.: The Effects of Coexposure to Extremes of Heat and Particulate Air Pollution on Mortality in California: Implications for Climate Change, American Journal of Respiratory and Critical Care Medicine, https://doi.org/10.1164/rccm.202204-0657OC, publisher: American Thoracic Society, 2022.

Raymond, C., Singh, D., and Horton, R. M.: Spatiotemporal Patterns and Synoptics of Extreme Wet-Bulb Temperature in the Contiguous United States, Journal of Geophysical Research: Atmospheres, 122, 13,108–13,124, https://doi.org/https://doi.org/10.1002/2017JD027140, _eprint: https://agupubs.onlinelibrary.wiley.com/doi/pdf/10.1002/2017JD027140, 2017.

https://doi.org/10.5194/egusphere-2025-4874
Preprint. Discussion started: 15 October 2025

Raymond, C., Matthews, T., and Horton, R. M.: The emergence of heat and humidity too severe for human tolerance, Science Advances, 6, eaaw1838, https://doi.org/10.1126/sciadv.aaw1838, publisher: American Association for the Advancement of Science Section: Research Article, 2020.

Raymond, C., Matthews, T., Horton, R. M., Fischer, E. M., Fueglistaler, S., Ivanovich, C., Suarez-Gutierrez, L., and Zhang, Y.: On the controlling factors for globally extreme humid heat, Geophysical Research Letters, 48, e2021GL096 082, 2021.

Rogers, C. D. W., Ting, M., Li, C., Kornhuber, K., Coffel, E. D., Horton, R. M., Raymond, C., and Singh, D.: Recent Increases in Exposure to Extreme Humid-Heat Events Disproportionately Affect Populated Regions, Geophysical Research Letters, 48, e2021GL094 183, https://doi.org/10.1029/2021GL094183, _eprint: https://onlinelibrary.wiley.com/doi/pdf/10.1029/2021GL094183, 2021.

Ryu, Y.-H. and Min, S.-K.: Long-term evaluation of atmospheric composition reanalyses from CAMS, TCR-2, and MERRA-2 over South Korea: Insights into applications, implications, and limitations, Atmospheric Environment, 246, 118 062, https://doi.org/10.1016/j.atmosenv.2020.118062, 2021.

Schnell, J. L. and Prather, M. J.: Co-occurrence of extremes in surface ozone, particulate matter, and temperature over eastern North America, Proceedings of the National Academy of Sciences, 114, 2854–2859, 2017.

Sherwood, S. C. and Huber, M.: An adaptability limit to climate change due to heat stress, Proceedings of the National Academy of Sciences, 107, 9552–9555, https://doi.org/10.1073/pnas.0913352107, publisher: National Academy of Sciences Section: Physical Sciences, 2010.

Sillman, S. and Samson, P. J.: Impact of temperature on oxidant photochemistry in urban, polluted rural and remote environments, Journal of Geophysical Research: Atmospheres, 100, 11 497–11 508, https://doi.org/10.1029/94JD02146, _eprint: https://onlinelibrary.wiley.com/doi/pdf/10.1029/94JD02146, 1995.

Sindelarova, K., Granier, C., Bouarar, I., Guenther, A., Tilmes, S., Stavrakou, T., Müller, J.-F., Kuhn, U., Stefani, P., and Knorr, W.: Global data set of biogenic VOC emissions calculated by the MEGAN model over the last 30 years, Atmospheric Chemistry and Physics, 14, 9317–9341, 2014.

Speizer, S., Raymond, C., Ivanovich, C., and Horton, R. M.: Concentrated and Intensifying Humid Heat Extremes in the IPCC AR6 Regions, Geophysical Research Letters, 49, e2021GL097 261, https://doi.org/10.1029/2021GL097261, _eprint: https://onlinelibrary.wiley.com/doi/pdf/10.1029/2021GL097261, 2022.

Strada, S., Fernández-Martínez, M., Peñuelas, J., Bauwens, M., Stavrakou, T., Verger, A., and Giorgi, F.: Disentangling temperature and water stress contributions to trends in isoprene emissions using satellite observations of formaldehyde, 2005–2016, Atmospheric Environment, 295, 119 530, 2023.

Tai, A. P. K., Mickley, L. J., and Jacob, D. J.: Correlations between fine particulate matter (PM2.5) and meteorological variables in the United States: Implications for the sensitivity of PM2.5 to climate change, Atmospheric Environment, 44, 3976–3984, https://doi.org/10.1016/j.atmosenv.2010.06.060, 2010.

Vecellio, D. J., Wolf, S. T., Cottle, R. M., and Kenney, W. L.: Evaluating the 35°C wet-bulb temperature adaptability threshold for young, healthy subjects (PSU HEAT Project), Journal of Applied Physiology, 132, 340–345, https://doi.org/10.1152/japplphysiol.00738.2021, publisher: American Physiological Society, 2022.

Vecellio, D. J., Kong, Q., Kenney, W. L., and Huber, M.: Greatly enhanced risk to humans as a consequence of empirically determined lower moist heat stress tolerance, Proceedings of the National Academy of Sciences, 120, e2305427 120, https://doi.org/10.1073/pnas.2305427120, publisher: Proceedings of the National Academy of Sciences, 2023.

Wagner, A., Bennouna, Y., Blechschmidt, A.-M., Brasseur, G., Chabrillat, S., Christophe, Y., Errera, Q., Eskes, H., Flemming, J., Hansen, K. M., Inness, A., Kapsomenakis, J., Langerock, B., Richter, A., Sudarchikova, N., Thouret, V., and Zerefos, C.: Comprehensive evalua-

https://doi.org/10.5194/egusphere-2025-4874
Preprint. Discussion started: 15 October 2025

tion of the Copernicus Atmosphere Monitoring Service (CAMS) reanalysis against independent observations: Reactive gases, Elementa: Science of the Anthropocene, 9, 00 171, https://doi.org/10.1525/elementa.2020.00171, 2021.

Weinberger, K. R., Harris, D., Spangler, K. R., Zanobetti, A., and Wellenius, G. A.: Estimating the number of excess deaths attributable to heat in 297 United States counties, Environmental Epidemiology, 4, e096, https://doi.org/10.1097/EE9.0000000000000096, 2020.

Westervelt, D. M., Horowitz, L. W., Naik, V., Tai, A. P. K., Fiore, A. M., and Mauzerall, D. L.: Quantifying PM2.5-meteorology sensitivities in a global climate model, Atmospheric Environment, 142, 43–56, https://doi.org/10.1016/j.atmosenv.2016.07.040, 2016.

Willers, S. M., Jonker, M. F., Klok, L., Keuken, M. P., Odink, J., van den Elshout, S., Sabel, C. E., Mackenbach, J. P., and Burdorf, A.: High resolution exposure modelling of heat and air pollution and the impact on mortality, Environment International, 89-90, 102–109, https://doi.org/10.1016/j.envint.2016.01.013, 2016.

Williams, J. E., Huijnen, V., Bouarar, I., Meziane, M., Schreurs, T., Pelletier, S., Marécal, V., Josse, B., and Flemming, J.: Regional evaluation of the performance of the global CAMS chemical modeling system over the United States (IFS cycle 47r1), Geoscientific Model Development, 15, 4657–4687, https://doi.org/10.5194/gmd-15-4657-2022, publisher: Copernicus GmbH, 2022.

Xu, Y., Wu, X., Kumar, R., Barth, M., Diao, C., Gao, M., Lin, L., Jones, B., and Meehl, G. A.: Substantial increase in the joint occurrence and human exposure of heatwave and high-PM hazards over South Asia in the mid-21st century, Agu Advances, 1, e2019AV000 103, 2020.

Zanis, P., Akritidis, D., Turnock, S., Naik, V., Szopa, S., Georgoulias, A. K., Bauer, S. E., Deushi, M., Horowitz, L. W., Keeble, J., Le Sager, P., O'Connor, F. M., Oshima, N., Tsigaridis, K., and van Noije, T.: Climate change penalty and benefit on surface ozone: a global perspective based on CMIP6 earth system models, Environmental Research Letters, 17, 024 014, https://doi.org/10.1088/1748-9326/ac4a34, publisher: IOP Publishing, 2022.

Zhai, S., Jacob, D. J., Wang, X., Shen, L., Li, K., Zhang, Y., Gui, K., Zhao, T., and Liao, H.: Fine particulate matter ($PM_{2.5}$) trends in China, 2013–2018: separating contributions from anthropogenic emissions and meteorology, Atmospheric Chemistry and Physics, 19, 11 031–11 041, https://doi.org/10.5194/acp-19-11031-2019, publisher: Copernicus GmbH, 2019.

Zhang, Y., Held, I., and Fueglistaler, S.: Projections of tropical heat stress constrained by atmospheric dynamics, Nature Geoscience, 14, 133–137, 2021.

Zheng, Y., Unger, N., Tadić, J. M., Seco, R., Guenther, A. B., Barkley, M. P., Potosnak, M. J., Murray, L. T., Michalak, A. M., Qiu, X., et al.: Drought impacts on photosynthesis, isoprene emission and atmospheric formaldehyde in a mid-latitude forest, Atmospheric Environment, 167, 190–201, 2017.